Polyhedron xxx (2013) xxx–xxx

Contents lists available at SciVerse ScienceDirect

Polyhedron

journal homepage: www.elsevier.com/locate/poly

Synthesis and characterization of 3d and 4f metal complexes of Schiff base ligands

Apoorva Upadhyay [a], Shefali Vaidya [a], Vakacharla S. Venkatasai [a], Prabha Jayapal [a], Anant K. Srivastava [c], Muralidharan Shanmugam [b,*], Maheswaran Shanmugam [a,*]

[a] Department of Chemistry, Indian Institute of Technology Bombay, Powai, Mumbai 400 076, Maharashtra, India
[b] Department of Chemistry, Northwestern University, Evanston, IL 60208, USA
[c] Department of Chemistry, Indian Institute of Science Education and Research, Pune 411 021, Maharashtra, India

ARTICLE INFO

Article history:
Available online xxxx

Keywords:
Schiff base
Lanthanide ion
Transition metal complex
EPR
DFT and TD-DFT calculations

ABSTRACT

Square planar complexes of monomeric $[Cu(L1)_2]$ (**1**) and $[Ni(L1)_2]$ (**2**) (where L1 is $C_{20}H_{24}NO_2$) are isolated through the use of Schiff base ligands and characterized by X-ray diffraction, UV–Vis, electron paramagnetic resonance (EPR) and DFT calculations. Effects of coordinating and non-coordinating solvent for **1** and **2** (UV–Vis) were studied in detail. The EPR spectra recorded for **1**, confirms the rhombic nature of Cu(II) ion of **1** in the solid state, g = [2.185, 2.086, 2.036], and frozen fluid with the spin Hamiltonian parameters, g = [2.207, 2.079, 2.040]. The slight deviation in the g-tensor of **1** from its powder to frozen solution is attributed to the loss of intermolecular hydrogen bonding in fluid solution. UV–Vis (for **1** and **2**) and EPR (for **1**) parameters obtained from DFT calculations are consistent with the experimental data, and further confirms that the solid state structures of **1** and **2** are maintained in solution. Crystal structures of praseodymium and lanthanum monomeric complexes obtained with HL2 ($C_{14}H_{11}NO_2$) are also reported. The X-ray crystal structure of the praseodymium complex solved in an orthorhombic crystal system with molecular formula $[Pr(HL_2)_2(NO_3)_3]$ (**3**), whereas lanthanum in a triclinic system with molecular formula $[La(HL_2)_3(NO_3)_3]$ (**4**) with multiple intermolecular hydrogen bonds. Complexes **3** and **4** are found to be in distorted bicapped square anti-prism and Icosahedron geometries respectively.

1. Introduction

Schiff bases are important in the fields of chemistry and biochemistry owing to their biological activities [1]. Apart from biological activities, Schiff base complexes have a wide range of applications. Photochromism is another characteristic of these materials leading to applications in various areas, such as the control and measurement of radiation intensity, display systems and optical computers [2]. The influence of steric hindrance on the electronic and structural properties of these complexes is explored by introducing bulky substituents into the existing skeleton of the molecule. Schiff bases are often used to stabilize unusual oxidation state of metal ions and provides good solubility in most of the solvents [3]. These metal complexes are of particular interest since they possess much better antibacterial activity than the metal-free ligands themselves, and also it can used as precursors to make various other metal complexes, just by exploiting the labile nature [1a]. In addition, Schiff base metal complexes often exhibits fascinating magnetic properties (Single Molecule Magnets; SMMs) since they contain 3d metal ions. Brechin and co-workers reported a family of Mn_6 cluster prepared by the use of oxime based Schiff base ligands, where the SMMs property is tuned by controlling the dihedral angle (twist angle) via ligand modification [4]. In an unrelated report Murugesu and co-workers have shown that just by modifying the substituent on the ligand, the geometry around monomeric cobalt changes which also drastically affects the single ion magnetic properties of cobalt monomeric complex [5]. The importance of the ligand field around the metal center is well established for Fe(II) and Co(II) complexes reported by Long and co-workers [6].

The magnetic properties shown by monomeric lanthanide complexes with Schiff base ligands are even more appealing. Due to strong intrinsic spin–orbit coupling usually lanthanide ions constitute an excellent source of anisotropy for building magnetic molecules. This has been strongly reflected in Ishikawa's terbium Pthalocyanin $[Tb(Pc)_2]^n$ (n = −1, 0 or +1) sandwich complexes, where even a single lanthanide ion exhibit out-of-phase susceptibility signal, which is of purely molecular origin. Not only that, the effective energy barrier shown by these monomers is the largest known for single ion magnets (SIM) [7]. In $[Tb(Pc)_2]^n$ Tb(III) exhibits near D_{4d} geometry, the latter along with axial elongation stabilizes the lowest J_z = ±6, which is responsible for the magnetic bi-stability. However, when the ligand field around Tb(III) is changed, and is described by general formula $(TbW_{10}O_{36})$ (D_{4d}), no

* Corresponding authors. Tel.: +91 22 2576 7187; fax: +91 22 2576 7152.
E-mail addresses: muralidharan.shanmugam@gmail.com (M. Shanmugam), eswar@chem.iitb.ac.in (M. Shanmugam).

0277-5387/$ - see front matter © 2013 Elsevier Ltd. All rights reserved.
http://dx.doi.org/10.1016/j.poly.2013.02.039

SMM properties are observed. The ligand field provided by polyoxometallates (POM) favors axial compression, which leads to $J_z = 0$ as ground state and $J_z = \pm 6$ becomes an excited state. However when Tb(III) is replaced by Erbium(III) ($ErW_{10}O_{36}$), the complex shows SMM behavior [8]. Followed by this discovery, several research groups are actively investigating the role of ligand field in determining the anisotropy and its structural correlation to the magnetization relaxation. Example of such studies are the organometallic Er(III) complex and acetyl acetonate complex studied by Gao and co-workers [9] and Dy(DOTA) complex by Sessoli and co-workers [10] Some of the monomeric Dy(III) single ion magnet shows three different relaxation pathways with one of the largest energy barrier reported for SIM, [11] but the U_{eff} is slightly lower than the Ishikawa's Tb(III) Phthalocyanin SIMs [7,12]. Very recently Coronado and co-workers has studied the magnetic behavior of lanthanide ions with formula $[LnP_5W_{30}O_{110}]$ under unusual C5 geometry. Under this geometry Dy(III) and Ho(III) show SMM properties [13]. It is very clear from the literature that the lanthanide ions under various ligand fields show distinct magnetic properties; however there are still no systematic investigations on this topic in order to have control over the anisotropy of the molecular cluster [14]. Also, the lanthanide-based SIMs reported using Schiff base ligands are relatively rare in literature. To understand thoroughly the ligand field effect (especially in lanthanide complexes), metal complexes (3d and 4f) with varying coordination numbers and geometries need to be isolated. In this work, we have investigated and reported new generation of 3d and 4f Schiff base complexes and their characterization by various spectroscopic methods.

2. Experimental

2.1. Materials and methods

Unless otherwise mentioned all the reactions were carried out under aerobic conditions. Analytical grade solvents and reagents were purchased from commercial sources (Alfa Aesar) and used without further purification. The elemental analyses (CHN) were carried out on a Thermoquest microanalyser. Infrared spectra were collected for the solid samples using KBr pellets on a Perkin-Elmer FT-IR spectrometer in 400 to 4000 cm^{-1} range. Electronic spectra were recorded on a Varian UV–Vis spectrophotometer in the range of 200–800 nm at room temperature. ESI-Mass spectrometry was performed using a Q-TOF micromass (YA-105) spectrometer. NMR data were collected on a Bruker Avance III 400 MHz instrument. Single crystal data were collected on a Bruker SMART CCD diffractometer (Mo Kα, $\lambda = 0.71073$ Å). In both cases the selected crystals were mounted on the tip of a glass pin using Paratone-N oil and placed in the cold flow produced with an Oxford Cryo-cooling device. Complete hemispheres of data were collected by using ω-scans (0.3 Å 30 s per frame). Integrated intensities were obtained with SAINT+ and they were corrected for absorption using SADABS. Structure solution and refinement was performed with the SHELX-package The structures were solved by direct methods and completed by iterative cycles of ΔF syntheses and full-matrix least-squares refinement against F. Variable temperature EPR spectra of solid and solution samples were recorded on a modified Varian E4 spectrometer operating at X-band (~9.5 GHz) and the EPR parameters (g and A tensors) are calculated using the Bruker Win-EPR SymFonia Software. TD-DFT calculations were performed by the GAUSSIAN 09 [15] software, whereas the EPR parameters (g tensor and the hyperfine) were calculated by ORCA 2.8 [16] program package. Since prediction of these parameters requires a reasonable estimation of spin density on the metal center, the employed exchange–correlations functional play a crucial role in computing these parameters. Hence the most popular hybrid B3LYP functional [17] in conjunction with TZVP [18] basis set for Ni, Cu and SVP for rest of the elements were used for EPR parameters and UV spectral calculations.

2.2. Synthesis of Schiff base ligand

The schematic route for making HL1 and HL2 is given in Scheme 1. The ligands were synthesized based on the reported method [19], but slightly modified to improve the yield of the product. 2-hydroxy-3-methoxy-benzaldehyde (*o*-vanillin) (4.0335 g, 0.0265 mol) was dissolved in 25 ml of ethanol in a 250 ml round bottom flask. Into this yellow solution 4–5 drops of acetic acid (catalytic amount) were added. The solution was stirred for 10 min. Equimolar amount of 2,6-diisopropylaniline (HL1) (5 ml, 0.0265 mol) or aniline (HL2) (2.416 ml, 0.0265 mol) was added into the above reaction mixture. The contents were heated under reflux for 24 h. Yellow crystals of HL1 were grown upon cooling the reaction mixture to room temperature. To isolate/crystallize HL2 as a solid, cold *n*-pentane was added into the ethanolic solution. The isolated crystals of both HL1 and HL2 were washed with *n*-hexane (3–4 times) and dried under vacuum. The formation and the purity of the ligand were confirmed by GC–MS HL1: (311 *m/z*) and NMR (see Supplementary info): ^{1}H NMR (400 MHz, Chloroform-d) δ 8.32 (s, 1H), 7.20 (s, 3H), 7.08–6.87 (m, 3H), 3.97 (s, 3H), 3.01 (hept, $J = 6.9$ Hz, 2H), 1.18 (d, $J = 6.9$ Hz, 12H). FT-IR (KBr pellet) 3444 cm^{-1} (m, $\nu_{(O-H)}$), 2962 cm^{-1} (s, $\nu_{(Ar-H)}$), 1621 cm^{-1} (s, $\nu_{(C=N)}$); yield = 7.42 g (90%). HL2: (227 *m/z*) and NMR (Supplementary Info): ^{1}H NMR (400 MHz, DMSO-d6) 3.83 (s, 1H), 8.96 (s, 1H), 7.52–7.38 (m, 4H), 7.37–7.21 (m, 2H), 7.14 (dd, $J = 8.0$, 1.4 Hz, 1H), 6.92 (t, $J = 7.9$ Hz, 1H). FT-IR (KBr pellet) 3440 cm^{-1} (m, $\nu_{(O-H)}$), 2923 cm^{-1} (s, $\nu_{(Ar-H)}$), 1614 cm^{-1} (s, $\nu_{(C=N)}$); yield = 5.41 g 90%).

2.3. Synthesis of $[M(L1)_2]$ [M = Cu (**1**) and Ni (**2**)]

The yellow ethanolic solution of HL1 (1.0 g, 3.215 mmol) was deprotonated using NaOH (0.128 g, 3.215 mmol). This solution was stirred for 10 min before adding the ethanolic solution of $CuCl_2{\cdot}2H_2O$ (0.274 g, 1.607 mmol) drop wise. During this addition, the color of the solution slowly turned from yellow to wine red. The reaction mixture was stirred continuously for another 18 h at room temperature. The wine red precipitate obtained from the reaction was filtered off and recrystallized using *n*-pentane. Single crystal, suitable for X-ray crystallography was grown within 2 days *Anal.* Calc. for $C_{40}H_{48}N_2O_4Cu$: C, 70.20; H, 7.07; N, 4.09. Found: C, 70.03; H, 7.08; N, 4.0%. FT-IR: 2957 cm^{-1} (s, $\nu_{(Ar-H)}$), 1602 cm^{-1} (s, $\nu_{(C=N)}$); yield: 0.791 g (72%).

For **2**, the synthetic procedure is the same as **1**, but $NiCl_2{\cdot}6H_2O$ was used instead of $CuCl_2{\cdot}2H_2O$. In this case the precipitate obtained was in green color. *Anal.* Calc. for $C_{40}H_{48}N_2O_4Ni$: C, 70.7; H, 7.12; N, 4.12. Found: C, 70.56; H, 7.11; N, 4.5%. FT-IR:

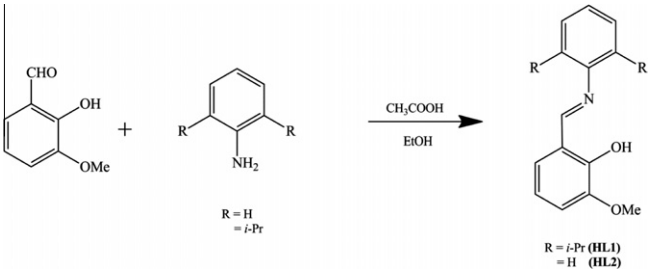

Scheme 1. General ligand synthetic scheme.

2958 cm^{-1} (s, $\nu_{(Ar-H)}$), 1605 cm^{-1} (s, $\nu_{(-C=N)}$); yield: 0.753 g (69%); ^1H NMR (400 MHz, Chloroform-d) δ: 7.37–7.18 (m, 2H), 7.12 (d, J = 7.6 Hz, 2H), 6.59 (dd, J = 7.9, 1.7 Hz, 1H), 6.42–6.26 (m, 2H), 4.50 (hept, J = 6.9 Hz, 2H), 3.19 (s, 3H), 1.41 (d, J = 6.9 Hz, 6H), 1.25 (d, J = 6.9 Hz, 6H).

2.4. Synthesis of $[Pr(L2)_2(NO_3)_3]$ (**3**) and $[La(L2)_3(NO_3)_3]$ (**4**)

To the 40 mL of ethanolic solution of HL2 (0.48 g, 0.0022 mol), 10 mL ethanolic solution of $Pr(NO_3)_3{\cdot}6H_2O$ (0.44 g, 0.0011 mol) was added drop wise. The resulting mixture was refluxed for 7–8 h. After completion of the reaction, the solvent was evaporated and the crude mixture was washed with diethyl ether. The obtained residue was recrystallized again from ethanol. Orange-red crystals of suitable quality for X-ray were obtained after 3 days at low temperature. IR data: 3447 cm^{-1} (m, $\nu_{(O-H)}$), 2925 cm^{-1} (s, $\nu_{(Ar-H)}$), 1632 cm^{-1} (s, $\nu_{(C=N)}$); yield: 0.454 g (30%).

Similar procedure as in 3 has been followed to make 4, but $La(NO_3)_3.6H_2O$ was used in place of $Pr(NO_3)_3{\cdot}6H_2O$. *Anal.* Calc. for **4**: C, 50.11; H, 3.90; N, 8.34. Found: C, 49.19; H, 3.69; N, 8.62%. IR data: 3446 cm^{-1} (m, $\nu_{(-OH)}$), 2922 cm^{-1} (s, $\nu_{(Ar-H)}$), 1631 cm^{-1} (s, $\nu_{(C=N)}$ yield: 0.359 g (27%).

3. Results and discussion

3.1. Synthesis and general characterization

Reaction of M(II) salt (M = Cu(II) or Ni(II)) with HL1 provides pure complex of **1** and **2** in good yield. The reaction of HL1 with various lanthanide salts under different conditions (temperature, solvents, and metal precursors) were not successful, confirmed by IR and NMR spectroscopy (data not shown); this could be possibly due to the steric hindrance provided by the isopropyl groups of HL1. To see the effect of steric hindrance, we prepared the HL2 ligand, by condensation of simple aniline with *o*-vanillin (Scheme 1). The reaction of Pr(III) or La(III) salts with HL2 led to the isolation of **3** and **4** respectively, The physical and chemical characterization of complexes **1**–**4** are detailed in following sections.

Crystals of **1**–**4** were isolated and infrared spectra were recorded in the solid state (KBr pellet). The IR spectra of metal-free ligand HL1 and HL2 show sharp peak at 1621 and 1614 cm^{-1} respectively which corresponds to azomethine (–C=N) group. The HL1's azomethine peak upon coordination with the copper(II) and nickel(II) ions significantly shifts to lower frequency by 19 and 16 cm^{-1}, respectively, thus confirming its binding to the metal(II) ions. A similar effect has been observed when HL2 is treated with Pr(III) or La(III) ion, however the peak moves to a higher frequency by 18 and 17 cm^{-1} respectively. The broad band around 3200 cm^{-1} for –OH group in metal-free ligand HL1 disappears in the metal complex (**1** and **2**) further supporting the complex formation. However, broad peak centered around 3440 cm^{-1} for the metal-free HL2 (ν_{-OH}) remains in the lanthanide complex with small shift in position (3447 cm^{-1}). ^1H NMR spectra were recorded for **1** and **2** in $CDCl_3$, whereas for **3** and 4 in deuterated DMSO. The observed spectral peaks are too broad for **1** due to the paramagnetic nature of Cu(II) ion, hence no analysis was performed. However, the ^1H NMR spectra of **2** shows sharp peaks. This indicates that **2** is likely to be diamagnetic in nature. In the metal-free ligand (HL1), the NMR peaks correspond to azomethine and other aromatic protons are observed in the region 8.32–6.87 ppm. These peaks are shifted considerably upfield (7.37–6.26 ppm) upon coordination with the nickel(II) ion. Similarly the peak at 3.97 ppm corresponds to the –OMe group of HL1 shifted upfield to 3.19 ppm. In HL1, the chemically equivalent isopropyl group shows a doublet peak at 1.18 ppm, which upon complexation with Ni(II) becomes chemically inequivalent, and splits into two doublets at 1.41 ppm, 1.25 ppm. The heptet shown by the CH-group (3.01 ppm in HL1) of isopropyl is significantly shifted downfield to 4.50 ppm upon complex formation (see Supplementary info (SFig. 1)). On the contrary, for **3** and **4**, the NMR spectra of these complexes exactly match with metal-free ligand peaks (HL2). This observation likely suggests that the solid state structures of **3** and **4** are not stable in solution or the metal-to-ligand interaction is not very strong (due to the shielding of the 4f orbital) or aromaticity of ligand is not disturbed considerably; hence the peaks are exactly matching with the metal-free ligand. For **1** and **2**, NMR and IR spectral data clearly confirms the formation of metal complexes. Significant changes in the IR peak positions of **3** and 4 substantiate the formation of lanthanide complexes, though there is no change in the NMR peak positions compared to the metal-free ligand.

3.2. Structural description of **1**–**4**

The reaction between the deprotonated ligand with the chloride precursors of Cu(II) and Ni(II) ion gives wine red and green color crystals, which are solved as monomeric complex with formulae $[Cu(L1)_2]$ (**1**) and $[Ni(L1)_2]$ (**2**), respectively. The crystal structures of **1** and **2** are shown in Fig. 1 and the crystallographic parameters are given in Table 1. In **1**, Cu(II) is found to be in distorted square planar geometry and its coordination sites are occupied by the phenolic oxygen of *o*-vanillin and the azomethine group of L1, which leaves the methoxy group of L1 as a non-coordinated site. Within this copper basal plane, the bond angles between N(11)–Cu(1)–N(51) and O(11)–Cu(1)–O(51) are found to be 146.25(14) and 153.07(13) respectively. Selected bond lengths and angles for **1** are given in Table 2. Detailed investigation of the packing diagram of **1** shows that there is intermolecular H-bonding between O(51) of one molecule and H(13′) of the second molecule; O(51)···H(13′) = 2.83 Å. In solid state **1**, behaves like a one-dimensional network due to H-bonding interaction.

Complex **2** crystallized in a triclinic system. Only half of the molecule is found in the asymmetric unit, the other half of the molecule is generated by inversion symmetry, where the inversion center pass through the Ni(II) ion. The coordination environment around the Ni(II) ion is square planar. Similar to **1**, the coordination sites are occupied again by phenolic oxygen and the azomethine group of L1. The bond angle between O(11)–Ni(1)–O(11)# and N(11)–Ni(1)–(N11)# (where # is symmetry equivalent of that atom) is 180° that indicates perfect square planar geometry for **2**. Selected bond lengths and bond angles for **2** are given in Table 2.

In the literature, several examples of lanthanide-based SMMs incorporate the *o*-vanillin ligand. The lanthanide-based SMMs with the highest reported energy barriers are Dy_4 (barrier 170 K) [20] and a Dy_6 cluster (barrier 200 K) [21] both of which are examples of *o*-vanillin complexes. We are interested in probing the coordination potential of *o*-vanillin-based ligands modified slightly with amines.

Reaction of HL2 with lanthanide(III) nitrate hexahydrate salt gives orange-red crystals. The analysis of single crystal X-ray data collected for these crystals showed the formation of monomeric $[Pr(HL2)_2(NO_3)_3]$ (**3**) and $[La(HL2)_3(NO_3)_3]$ (**4**). The thermal ellipsoid X-ray structures of **3** and **4** are shown in Fig. 1.

Their corresponding crystallographic parameters are shown in Table 1. Complex **3** crystallized in an orthorhombic space group. From Fig. 1C it is very clear that, there are two ligands which partially complete the coordination sites of Pr(III) ion. Given the oxophillic nature of lanthanides, it is explicable that the coordination sites are filled by phenolic oxygens and the oxygen atom of the methoxy group in vanillin, which leaves the azomethine group in HL2 free of binding. In **3**, Pr(III) shows coordination number of

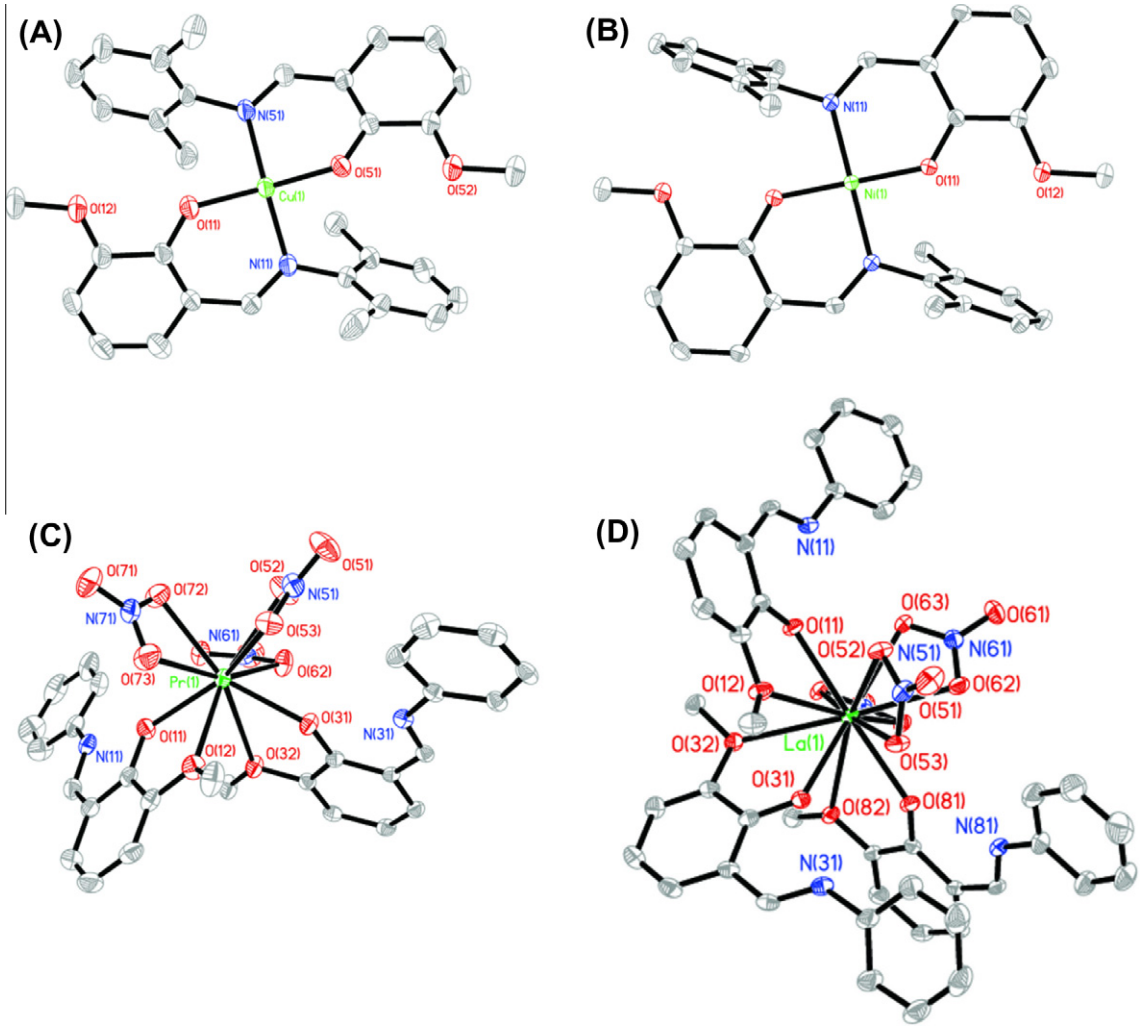

Fig. 1. (A–D) Crystal structures of **1–4** respectively. Color code: green = Cu(II) or Ni(II) or Pr(III) or La(III); red = O; blue = N; grey = C. Side chain carbon and hydrogen atoms are removed for clarity in **1–4**. (Color online.)

Table 1
Crystallographic parameters for **1–4**.

	1	**2**	**3**	**4**
Formula	$CuC_{40}H_{48}N_2O_4$	$C_{40}H_{48}N_2NiO_4$	$C_{28}H_{26}N_5O_{13}Pr$	$C_{42}H_{39}N_6O_{15}La$
Size (mm)	0.17 × 0.15 × 0.12	0.18 × 0.15 × 0.11	0.2 × 0.15 × 0.15	0.18 × 0.12 × 0.08
System	monoclinic	triclinic	orthorhombic	triclinic
Space group	C2/c	$P\bar{1}$	*Pbca*	$P\bar{1}$
a (Å)	30.341(7)	8.9526(13)	9.7726(6)	11.1517(13)
b (Å)	10.908(2	9.9901(14)	17.2379(10)	11.8908(14)
c (Å)	24.087(6)	10.4529(16)	36.279(2)	16.396(2)
α (°)	90	109.968(2)	90	81.998(2)
β (°)	115.412(9)°	91.134(3)°	90	79.795(2)
γ (°)	90	93.020(3)°	90	79.563(2)
V (Å^3)	7200(3)	876.7(2)	6111.5(6)	2091.4(4)
Z	8	1	8	2
ρ_{calc} (g/cm^{-3})	1.263	1.287	1.699	1.599
$2\theta_{max}$	54.22	56.72	53.46	56.88
Radiation	Mo Kα	Mo Kα	Mo Kα	Mo Kα
λ (Å)	0.71073	0.71073	0.71073	0.71073
T (K)	100	100	100	100
Reflections	43474	10702	95002	31973
Independent reflections	7796	4369	6481	10453
Reflections with [$I > 2\sigma(I)$]	5356	6889	5346	8141
R_1	0.0650	0.0310	0.0308	0.0332
wR_2	0.1824	0.0775	0.0639	0.0690

Table 2
Selected bond angles and bond lengths for **1** and **2**.

Bond length (Å)	1	Bond length (Å)	2
Cu(1)–O(11)	1.868(2)	Ni(1)–O(11)	1.8274(10)
Cu(1)–O(51)	1.866(2)	Ni(1)–N(11)	1.9115(11)
Cu(1)–N(51)	1.978(3)		
Cu(1)–N(11)	1.961(3)		
Bond angle (°)	**1**	**Bond angle (°)**	**2**
O(11)–Cu(1)–O(51)	153.07(13)	O(11)#1–Ni(1)–O(11)	180.0
O(11)–Cu(1)–N(51)	94.03(11)	O(11)#1–Ni(1)–N(11)#1	93.11(4)
O(51)–Cu(1)–N(51)	93.25(11)	O(11)–Ni(1)–N(11)#1	86.89(4)
O(11)–Cu(1)–N(11)	94.38(11)	N(11)#1–Ni(1)–N(11)	180.00(6)
O(51)–Cu(1)–N(11)	93.84(11)		
N(51)–Cu(1)–N(11)	146.25(14)		

10, four of them are occupied by the HL2 ligand and the rest of the sites are filled by three nitrate ions. Complex **3** exhibits a distorted bi-capped square anti-prism geometry (Fig. 2).

On the contrary, **4** crystallized in a triclinic system with a $P\bar{1}$ space group. There are two molecules found in the asymmetry unit, which are crystallographically inequivalent. X-ray structural investigation reveals that there are three HL2 ligands in **4**, as compared to 2 HL2 ligands in **3**.

This could possibly be due to the increase in ionic radii of La(III) (1.032 Å) compared to Pr(III) (0.99 Å) [22], which allows the additional ligand to be bound to the La(III) ion. All three nitrates and two of HL2 ligands show similar coordination modes around La(III) as in **3**, however, the additional ligand provides extra coordination through both the phenolic oxygen and the methoxy group, which results in expansion of coordination number from 10 to 12 for **4** as compared to **3**. This keeps the La(III) ion in distorted icosahedron geometry (Fig. 2).

In **3** and **4**, both lanthanide ions exist in the 3+ oxidation state, and their cationic charges are neutralized by three nitrate groups and this scenario further confirms that ligands remain protonated. However, the proton from phenolic oxygen is migrated to the azomethine nitrogen atom, forms zwitter ionic ligand. A similar behavior is reported for a monomeric Dy(III) complex prepared with a different Schiff base ligand [23]. Selected bond lengths for **3** and **4** are shown in Table 3.

Detailed investigation of packing diagrams of **3** and **4** shows the existence of multiple both intra and intermolecular hydrogen bonds network. The intermolecular hydrogen bonding is facilitated by the terminal oxygen of various nitrate groups with aromatic protons of another molecule, whereas the migrated proton attached to the azomethine enables the intra-molecular hydrogen bonding with the methoxy group of vanillin.

The atoms involved in hydrogen bonding and their corresponding distances are shown in Table 4 for both complexes. Further DFT calculations have been performed to understand the electronic structure and spectroscopic parameters of complexes **1** and **2**. The calculated structural parameters (DFT optimized structure of **1** and **2**) are in good agreement to the X-ray structure and thus we have computed the absorption and EPR properties of these complexes.

3.3. UV–Vis absorption studies of *1* and *2*

To understand the electronic structure of **1** and **2**, UV–Vis spectra were recorded for these complexes (in CH_2Cl_2 (DCM), CH_3CN and DCM/pyridine mixture) and metal-free ligand (DCM), in the range of 200–800 nm. The absorption at 338 nm for the ligand is

Table 3
Interatomic distance between M(III) to ligated atoms (Å) in **3** and **4** (where M = Pr(III) (**3**) or La(III) (**4**).

Pr(1)–O(11)	2.624(2)	La(1)–O(11)	2.4786(19)
Pr(1)–O(12)	2.367(2)	La(1)–O(12)	3.0047(19)
Pr(1)–O(31)	2.727(2)	La(1)–O(31)	2.462(2)
Pr(1)–O(32)	2.403(2)	La(1)–O(32)	2.866(2)
Pr(1)–O(51)	2.593(2)	La(1)–O(52)	2.6857(19)
Pr(1)–O(53)	2.607(2)	La(1)–O(53)	2.677(2)
Pr(1)–O(62)	2.660(2)	La(1)–O(62)	2.657(2)
Pr(1)–O(63)	2.532(2)	La(1)–O(63)	2.665(2)
Pr(1)–O(72)	2.545(2)	La(1)–O(72)	2.7202(18)
Pr(1)–O(73)	2.545(2)	La(1)–O(73)	2.6174(19)
		La(1)–O(81)	2.4987(19)
		La(1)–O(82)	3.078(14)

Table 4
Inter and intra molecular hydrogen bonding between the atoms in **3** and **4** (Å).

Complex **3***		Complex **4***	
D–H···A	d(D···A)	D–H···A	d(D···A)
C(17)–H(17)···O(72)#1	3.333(4)	C(17)–H(17)···O(52)#1	3.182(3)
C(19)–H(19)···O(71)#1	3.252(5)	C(23)–H(23)···O(51)#1	3.406(4)
C(14)–H(14)···O(52)#2	3.377(4)	C(87)–H(87)···O(72)#2	3.406(3)
C(37)–H(37)···O(62)#3	3.356(4)	C(91)–H(91)···O(61)#3	3.379(4)
C(39)–H(39)···O(62)#3	3.429(4)	N(11)–H(11N)···O(11)	2.654(3)
C(32)–H(32)···O(61)#3	3.492(4)	N(11)–H(11N)···O(63)	3.254(3)
C(24)–H(24B)···O(61)#4	3.228(4)	N(31)–H(31N)···O(31)	2.522(3)
N(31)–H(31)···O(32)	2.593(3)	N(81)–H(81N)···O(81)	2.619(3)
N(11)–H(11)···O(12)	2.606(3)		

* Symmetry transformations used to generate equivalent atoms: For 3: #1 $-x+3/2$, $y-1/2$, z #2 $-x+1/2$, $y-1/2$, z #3 $x-1/2$, y, $-z+1/2$, #4 $x-1$, y, z. For **4** #1 $-x+1$, $-y+1$, $-z$ #2 $-x+1$, $-y$, $-z+1$ #3 $-x+1$, $-y+1$, $-z+1$.

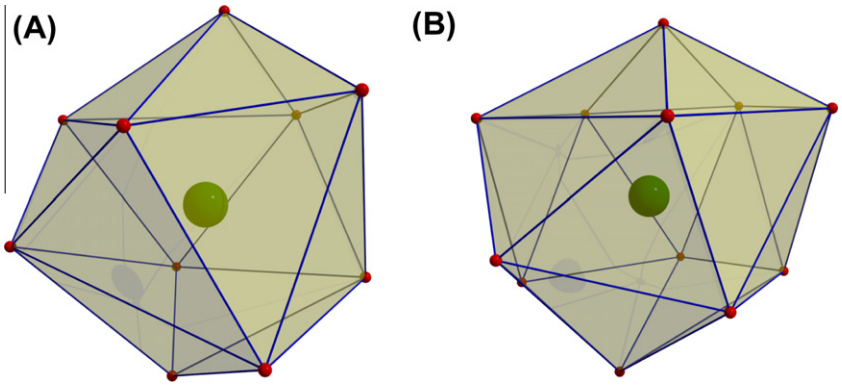

Fig. 2. (A) Polyhedral view of complex **3** in distorted bicapped square anti-prism geometry (B) complex **4** in distorted icosahedral geometry.

attributed to an n–π^* transition between lone-pair electrons of the *p* orbitals of the N atom in the azomethine (HC = N) group [24]. The sharp peaks at 268 nm and 222 nm are assigned to the π–π^* transitions of the Schiff base.

The X-ray crystal structure analysis shows that **1** and **2** have four-coordinate square planar structures and several similar types of monomeric Schiff base complexes of M(II) (M = Cu and Ni) ions are available in the literature. In the presence of suitable solvent(s), these metal-ion complexes change their coordination number, usually from four coordinate to five or six. In this line of interest, Elias et al. studied the change in Lewis acidity of tetra-coordinated Cu(II) ion in the presence of pyridine and the ligand substituents effect, where the change of geometry around Cu(II) ion was well witnessed [25]. In an unrelated report, Yamda has also shown that Cu(II) ion changes its four coordinate geometry to five or six coordination geometry [26]. The electronic structure of Cu(II) ion allows such kind of changes. Similarly evidence has been shown for change of geometry of Ni(II) ions from square planar geometry to octahedral geometry [26,27]. In order to see whether **1** and **2** are susceptible to changes of their coordination numbers in the presence of a suitable solvent, we have recorded UV–Vis spectra for **1** and **2** in DCM (non-coordinating), acetonitrile (coordinating) and also pyridine. (pyridine/DCM) (Supplementary info; SFig. 3).

In DCM **1** shows three distinct bands at 231 nm, 276 nm and a broad band around 350–400 nm (Fig. 3). This broad band is attributed to the ligand to metal charge transfer (LMCT). The bands were observed below 300 nm which is the characteristic signature of ligand to ligand charge transfer transition (π–π^*) [24]. The d–d transition is extremely weak which is expected to be above 400 nm. When UV–Vis spectrum was recorded in CH_3CN, no significant change is observed, when compared to the spectrum recorded in DCM, except that some of the CT bands, which correspond to ligand are merged together. The spectrum of **1** dissolved in DCM with 2 equivalents of pyridine essentially looks similar to spectra recorded in DCM (Supplementary info).

All these observations suggest that **1** is not susceptible to changes in its coordination geometry/number due to solvent effect.

For **2** (in DCM), there are bands at 230, 268 nm and broad bands around 305–365 nm and 420–460 nm (Fig. 4). All these bands are assigned to both MLCT and LMCT. As observed in the case of 1, there is no such solvent dependent effect on the coordination geometry of 2.

The substituents, namely 2,6-diisopropyl groups (L1) present in **1**, provide a substantial steric hindrance, which often does not allow the external ligands, including solvents, to access the available coordination site(s) in the Cu(II) ion and, hence no expansion of coordination number takes place. Therefore it is conceivable that there is no significant change in the UV spectrum of **1**, in all solvents (CH_3CN, DCM and pyridine), particularly in d-d transition, even though electronic configuration of **1**, allows geometry changes (d^9 system, Jahn–Teller distortion). Most importantly, the M(II) ion (M = Cu, Ni) prefers to stay in four coordination geometry, due to the strong ligand field effects which been observed previously in a similar Schiff-base Cu(II) complex; for example, the four coordinated copper(II)-Schiff base complex, synthesized by the condensation of ethylenediammine and formyl group, followed by metalation showed no solvent effects (less steric hindrance compared to 1) and hence no change in coordination geometry, due to the strong ligand field effects that arise from the Schiff-base ligand. [26,28] The strong ligand field effects of L1 combined with the steric hindrance provided by the diisopropyl groups is likely to prevent the expansion of coordination geometry of **1**, which is equally applicable to **2**.

TD-DFT calculations were performed on **1** and **2** to compute the UV–Vis spectra to validate the tentative spectral assignment. The computed spectra along with the assignments are shown in Figs. 3

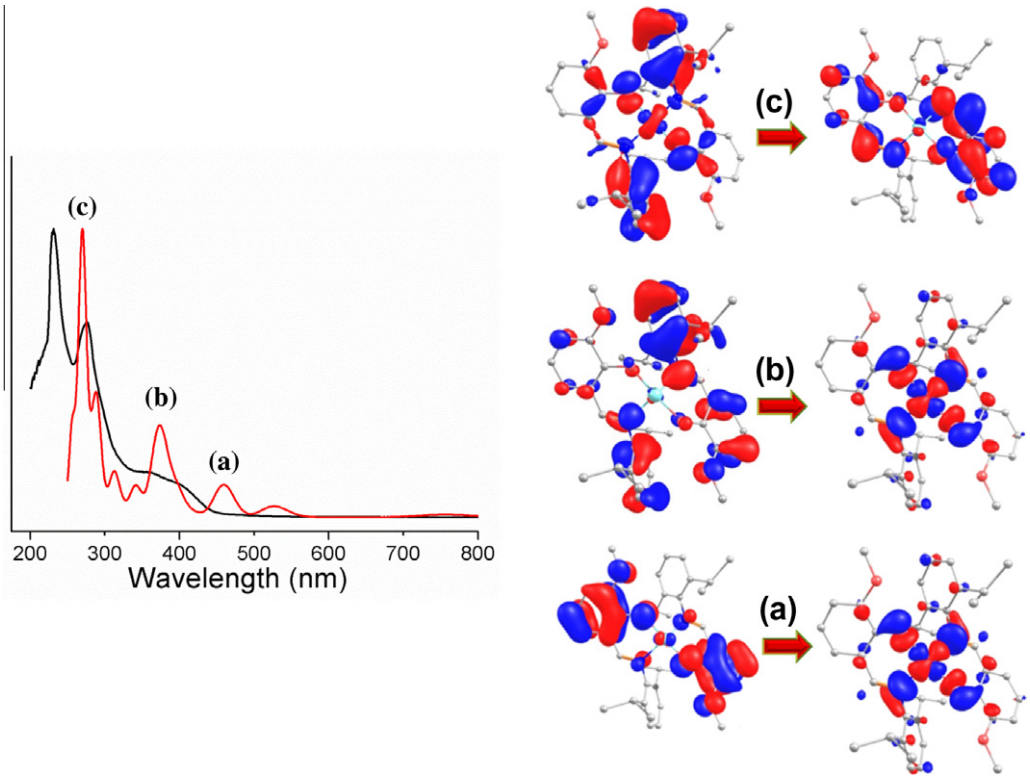

Fig. 3. Normalized UV–Vis spectra recorded in DCM (black) for **1**. Red line represents the calculated UV–Vis spectrum from TD-DFT calculations for **1**. The orbitals involved in transition shown in the right panel of the figure and their peak corresponds to the transition is labeled with a, b, and c. (Color online.)

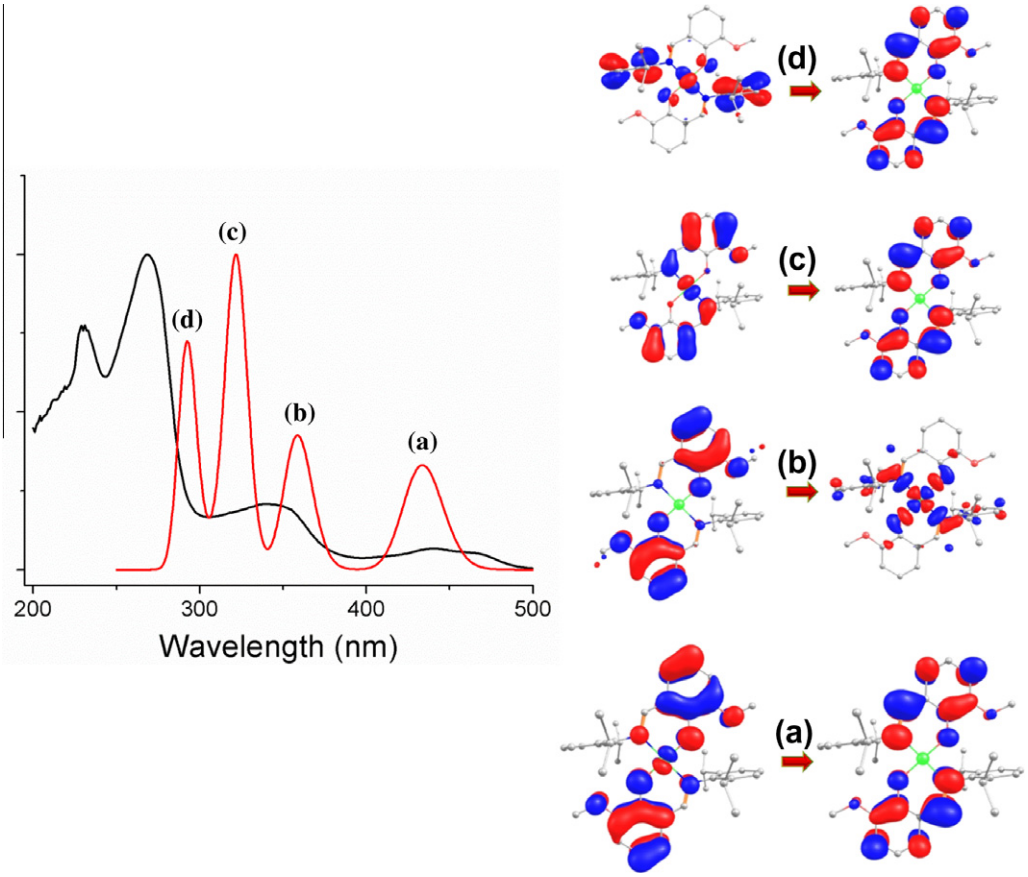

Fig. 4. Normalized UV–Vis spectra recorded in DCM (black) for **2**. Red line represents the calculated UV–Vis spectrum from TD-DFT calculations for **2**. The orbitals involved in transition shown in the right panel of the figure and their peak corresponds to the transition is labeled with a, b, c and d. (Color online.)

and 4. For **1**, the band centered around 459 nm is a d–d transition and this band is extremely weak in the experimental spectrum. The band which appears at 377 nm is attributed to LMCT, while the most intense band at 277 nm is MLCT. For complex **2** (Fig. 4), all the computed bands are CT in nature with bands centered around 433, 321 and 294 nm are being MLCT (doubly occupied d-orbitals to π^* orbitals of the coordinated atoms) bands, while the transition centered around 359 nm is LMCT (π orbital of the ligand to $d_{x^2-y^2}$ orbital of Ni(II)). The TD-DFT computed spectrum for **1** nicely reproduces the experimental results, confirming our spectral assignments, however for **2**, the calculated bands are slightly shifted towards higher wavelength.

3.4. Electron paramagnetic resonance studies of *1* and *2*

Fig. 5 shows the EPR spectra of poly-crystalline, fluid and frozen samples of **1** recorded at room temperature (RT) and 77 K, respectively on a modified Varian-E4 spectrometer operating at X-band (~9.5 GHz) frequency. The EPR spectra of poly-crystalline sample of **1** at RT, as well as at 77 K show only rhombic EPR signal (Fig. 5A), whereas the fluid and frozen (toluene) solutions of **1** show nicely resolved hyperfine structures, arising from ^{63,65}Cu (I = 3/2) and ^{14}N (I = 1) nuclei of 1 (Fig. 5B).

The lack of fine structures in the polycrystalline EPR spectra of **1** is likely due to either exchange interaction between the paramagnetic molecules or possible involvement of H-bonding interaction (O(51)–H(13′)). The absence of the half-field signal at the low magnetic field (~1600–1700 G) in the EPR spectra of **1** at both RT and 77 K (ΔM_S = 2 transition), rules out strong Cu–Cu interaction, consistent with X-ray crystal structure of the mononuclear complex, **1**. The polycrystalline EPR spectra are simulated nicely with the rhombic g-tensor, g = [2.19,2.099,2.036] and the simulated values are consistent with the molecular geometry and within the range reported for mononuclear copper(II) complexes with N_2O_2 coordination geometry [29]. The observation of $g_z > g_x > g_y$ also confirms that **1** possess a $(dx^2-y^2)^1$ ground orbital state. The fluid solution EPR spectrum of **1** shows a nicely resolved four-line hyperfine pattern due to the electron spin interaction (S = ½) with the nuclear spin of $I(^{63,65}\text{Cu})$ = 3/2, centered at g_{iso} = 2.11 with the isotropic hyperfine coupling of $a_{iso}(^{63,65}\text{Cu})$ = 74 G. However, no super hyperfine structure from the two coordinated nitrogen ligands of L1 is observed at RT, possibly due to the large EPR line widths that overcome the weak hyperfine coupling of ^{14}N-nuclei of **1**. The observed strongly differing EPR line widths of the four-line pattern arising from Cu(II) ion can be predominately attributed to well characterized slow-tumbling phenomena [30]. As shown in Fig. 5, the spectrum is simulated nicely with the spin-Hamiltonian parameters given in Table 5. The frozen solution EPR spectrum of **1** at 77 K show super hyperfine structure from the two coordinated ^{14}N ligands of L1, in addition to strong hyperfine coupling from ^{63,65}Cu(II) ion. The frozen solution EPR spectrum is nicely reproduced with the following spin-Hamiltonian parameters; g = [2.207,2.079,2.04], $\boldsymbol{A}(^{63,65}\text{Cu})$ = [188,15,15] G, a_{iso} (^{63,65}Cu) = 72.7 G, $\boldsymbol{A}(^{14}\text{N})$ = [2,19,2] G, line widths = [24,12,12] G. The observation of ^{14}N super hyperfine structure confirms its coordination to the Cu(II) ion.

The average g and $a_{iso}(^{63,65}\text{Cu})$ calculated from the simulation of frozen solution EPR spectrum is in good agreement with the value extracted from the simulation of fluid solution EPR spectrum, thus the extracted spin-Hamiltonian parameters (Table 5) are

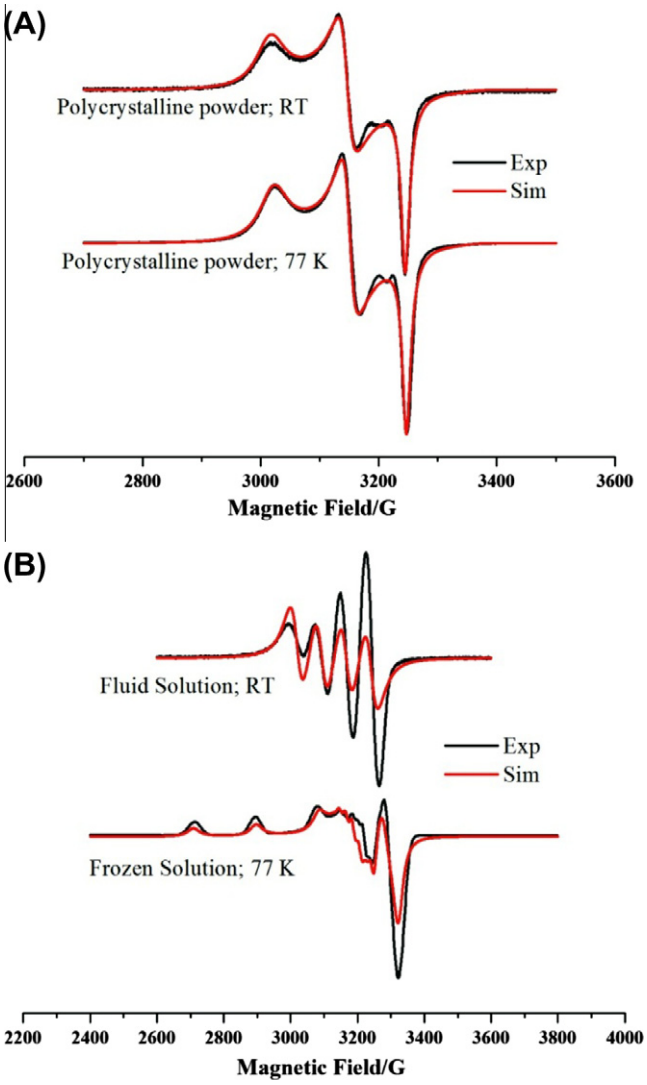

Fig. 5. X-band EPR spectra of **1**; (A) polycrystalline powder measured at RT (top) and 77 K (bottom); (B) solution in toluene measured at RT (top) and 77 K (bottom). The red lines are corresponding simulations. *Conditions;* MA = 5 G, average microwave frequency = 9.25 GHz, time constant = 300 ms, scan time = 4 min, Temp = RT or 77 K. (Color online.)

consistent with the X-ray crystal structure of **1** and demonstrate that the planar structure of **1** in the solid state, as revealed from X-ray crystal structure, is maintained in the fluid and frozen solution states. The extracted *g* and *A* tensors (Table 5) are typical of mononuclear copper complexes with N_2O_2 coordination geometry [29]. It is noteworthy that the shape of the polycrystalline EPR spectrum is distinctly different from the fluid and frozen solution spectra of **1**. In the same vein the extracted *g*-tensor also varies slightly, especially at magnetic fields near g_1 and g_2. The striking difference between the two states is likely due to the possible loss of H-bonding interaction in the fluid/frozen state, but the planarity of **1** is maintained in both fluid and frozen solutions.

Complex **2** remains EPR silent in solid state (RT and 77 K), in toluene (room temperature and 77.0 K) as well as in the presence of coordinating solvent (two equivalent of pyridine in toluene) suggests that Ni(II) maintains it square planar structure and possesses a singlet ground state. Majority of the magnetic properties reported for the metal complexes are investigated in solid state, and the researcher investigate the anisotropy in solid state alone. However, the studies of anisotropy changes, of monomeric complexes in solution, are relatively rare including monomeric complexes. In order to study the effect of solvent on the anisotropy of the Ni(II) ions, the steric hindrance will need to be relaxed (compare to **2)** systematically. This work is currently in progress.

To extract the *g* and *A*-tensors DFT calculations have been performed on **1**, which are given in Table 5 and the computed spin density plot is given in Fig. 6. As expected the unpaired electron is located in the $d_{x^2-y^2}$ orbital, but it has significant contribution from the d_{xy} orbital and this is essentially due to the distorted structure of **1** with the twist angle of 39.4°. Spin density of 0.565 has been noted on Cu(II) while the coordinated O and N atoms have ~0.1, indicating a strong delocalization of the unpaired electron onto the ligand orbitals. Computed EPR *g*-tensors are in line with the experimental observation .i.e. $g_z > g_x$, g_y and this trend is expected for unpaired electrons located in the $d_{x^2-y^2}$ orbital.

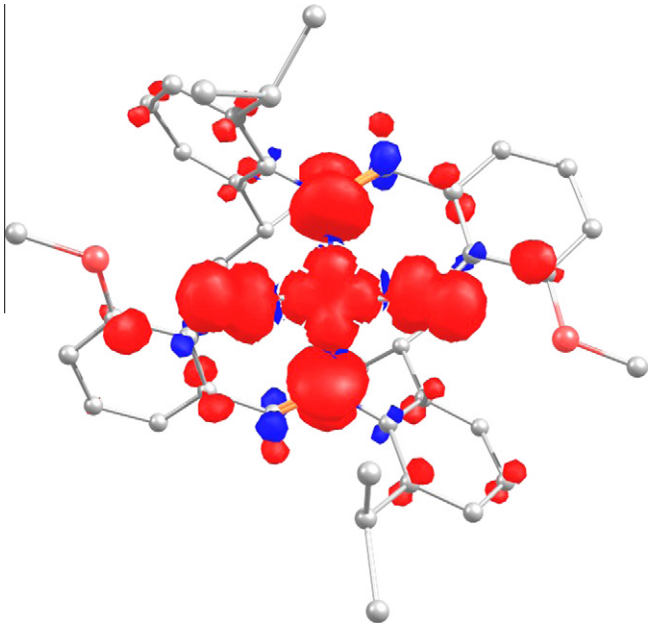

Fig. 6. Spin density distribution of **1** from DFT calculation. Red and blue represent positive and negative spin densities respectively. (Color online.)

Table 5
Simulation of experimental and DFT calculated spin Hamiltonian parameters (*g* and hyperfine tensors) for **1**.

Compound	*g*- and *A*-tensors of **1**			
	g-tensor/g_{ave}	A(^{63,65}Cu)/G	A(^{14}N)	Line widths (G)
Polycrystalline (RT)	[2.19, 2.099, 2.036]/2.108	N/A	N/A	[34, 19, 10]
Polycrystalline (77 K)	[2.185, 2.086, 2.036]/2.102	N/A	N/A	[34, 17, 10]
Fluid Solution (RT)	2.11	74	N/A	42
Frozen Solution (77 K)	[2.207, 2.079, 2.04]/2.109	[188, 15, 15]	[2, 20, 2]	[25, 13, 13]
DFT	[2.147, 2.056, 2.031/2.078	[−171.6, −33.4, −2.6]	[35.6, 45.1, 34.2,]	–

Although the computed *g*-tensors trend is in agreement with the experiment, the absolute magnitude is underestimated compared to experiments and this is essentially due to the overestimation of covalency of Cu(II) by the employed exchange–correlation functional [31]. Moreover the computed copper hyperfine tensor is in agreement with the experimental values (frozen solution). The computed nitrogen super-hyperfine lines, particularly A_x and A_y are overestimated compared to experimental observation.

3.5. Magnetic properties of **3** and **4**

Preliminary results on **3** and **4** suggest that the steric hindrance plays an important role in the isolation of various lanthanide monomeric complexes. We are in the process of isolating analogous monomeric complexes of other lanthanide ions with HL2. Though influence of ligand field is very minimal in lanthanide complexes, it does have significant contribution in determining the anisotropy of the resultant molecule. Hence detailed electronic and magnetic properties of these lanthanide complexes and effect of ligand field to the magnitude of anisotropy will be investigated in detail (for **3**, **4** and the other analogous complexes) which will be communicated in the near future.

4. Conclusions

We have reported monomeric Cu(II) and Ni(II) complexes incorporating Schiff-base ligands. Solvent has no influence on the coordination geometry of both **1** and **2**, due to the strong ligand field effects of L1, in addition to the steric hindrance provided by the isopropyl groups, as evidenced from UV–Vis and EPR spectroscopic studies. EPR spectra recorded on the polycrystalline and fluid solution of **1** and its corresponding spin Hamiltonian parameters are consistent with the rhombic nature of the Cu(II) ion found in the X-ray crystal structure of **1**. Significant deviation occurs between the EPR spectra of 1 in solid state and the ones of fluid or frozen solution; this is attributed to the intermolecular hydrogen bonding formation. The EPR parameters calculated for **1** from DFT calculation are in good agreement with the experimental tensors, further supporting the electronic structure of Cu(II) ion in **1**. Complex **2** remains EPR silent in coordinating solvent, which shows that the Ni(II) ion maintains its solid state structure even in solution. The coordination efficiency of the modified vanillin-based ligands was tested and the preliminary results obtained with HL2 look promising and the isolated solid state structures of lanthanide complexes of Pr(III) and La(III) (**3** and **4**) are presented. Their solid and solution state magnetic properties are currently under detailed investigation.

Acknowledgements

MS would like to acknowledge DST (SR/S1/IC-32/2011), DST nanomission (SR/NM/NS-1119/2011) India and IIT, Bombay for financial support. MS likes to thank Prof. G. Rajaraman (IIT Bombay) for helpful discussions and to Prof. Boomishankar R (IISER, Pune) for collection of crystal data. AU and SV acknowledge CSIR, India for fellowship. PJ would like to thank DST-India for the FAST TRACK young scientist fellowship (SR/FT/CS-56/2011).

Appendix A. Supplementary data

CCDC 916045, 916046, 916656 and 916657 contain the supplementary crystallographic data for **1**–**4**. These data can be obtained free of charge via http://www.ccdc.cam.ac.uk/conts/retrieving.html, or from the Cambridge Crystallographic Data Centre, 12 Union Road, Cambridge CB2 1EZ, UK; fax: +44 1223 336 033; or e-mail: deposit@ccdc.cam.ac.uk. Supplementary data associated with this article can be found, in the online version, at http://dx.doi.org/10.1016/j.poly.2013.02.039.

References

[1] (a) H.F. Abd El-Malim, M.M. Omar, G.G. Mohamed, M.A. El-Ela Sayed, Eur. J. Chem. 2 (2011) 178;
(b) M. Manjunatha, V.H. Naik, A.D. Kulkarni, S.A. Patil, J. Coord. Chem. 64 (2011) 4264;
(c) R.N. Patel, A. Singh, K.K. Shukla, V.P. Sondhiya, D.K. Patel, Y. Singh, R. Pandey, J. Coord. Chem. 65 (2012) 1381;
(d) R.N. Patel, A. Singh, V.P. Sondhiya, Y. Singh, K.K. Shukla, D.K. Patel, R. Pandey, J. Coord. Chem. 65 (2012) 795;
(e) T. Takeuchi, A. Boettcher, C.M. Quezada, M.I. Simon, T.J. Meade, H.B. Gray, J. Am. Chem. Soc. 120 (1998) 8555;
(f) M.-J. Xie, X.-D. Yang, W.-p. Liu, S.-p. Yan, Z.-h. Meng, J. Inorg. Biochem. 104 (2010) 851;
(g) J. Zuo, C. Bi, Y. Fan, D. Buac, C. Nardon, K.G. Daniel, Q.P. Dou, J. Inorg. Biochem. 118 (2013) 83.
[2] (a) C.-M. Che, C.-C. Kwok, S.-W. Lai, A.F. Rausch, W.J. Finkenzeller, N. Zhu, H. Yersin, Chem.-Eur. J. 16 (2010) 233;
(b) Z. Guo, W.-L. Tong, M.C.W. Chan, Chem. Commun. (2009) 6189;
(c) C.J. Whiteoak, G. Salassa, A.W. Kleij, Chem. Soc. Rev. 41 (2012) 622.
[3] D. de Bellefeuille, M.S. Askari, B. Lassalle-Kaiser, Y. Journaux, A. Aukauloo, M. Orio, F. Thomas, X. Ottenwaelder, Inorg. Chem. 51 (2012) 12796.
[4] (a) R. Inglis, J. Bendix, T. Brock-Nannestad, H. Weihe, E.K. Brechin, S. Piligkos, Chem. Sci. 1 (2010) 631;
(b) R. Inglis, E. Houton, J. Liu, A. Prescimone, J. Cano, S. Piligkos, S. Hill, L.F. Jones, E.K. Brechin, Dalton Trans. 40 (2011) 9999;
(c) L.F. Jones, M.E. Cochrane, B.D. Koivisto, D.A. Leigh, S.P. Perlepes, W. Wernsdorfer, E.K. Brechin, Inorg. Chim. Acta 361 (2008) 3420;
(d) C.J. Milios, R. Inglis, A. Vinslava, R. Bagai, W. Wernsdorfer, S. Parsons, S.P. Perlepes, G. Christou, E.K. Brechin, J. Am. Chem. Soc. 129 (2007) 12505;
(e) C.J. Milios, A. Vinslava, W. Wernsdorfer, A. Prescimone, P.A. Wood, S. Parsons, S.P. Perlepes, G. Christou, E.K. Brechin, J. Am. Chem. Soc. 129 (2007) 6547.
[5] T. Jurca, A. Farghal, P.-H. Lin, I. Korobkov, M. Murugesu, D.S. Richeson, J. Am. Chem. Soc. 133 (2011) 15814.
[6] (a) D.E. Freedman, W.H. Harman, T.D. Harris, G.J. Long, C.J. Chang, J.R. Long, J. Am. Chem. Soc. 132 (2010) 1224;
(b) J.M. Zadrozny, M. Atanasov, A.M. Bryan, C.-Y. Lin, B.D. Rekken, P.P. Power, F. Neese, J.R. Long, Chem. Sci. 4 (2013) 125;
(c) J.M. Zadrozny, J.R. Long, J. Am. Chem. Soc. 133 (2011) 20732.
[7] (a) N. Ishikawa, M. Sugita, T. Ishikawa, S. Koshihara, Y. Kaizu, J. Phys. Chem. B 108 (2004) 11265;
(b) N. Ishikawa, M. Sugita, T. Ishikawa, S.-Y. Koshihara, Y. Kaizu, J. Am. Chem. Soc. 125 (2003) 8694;
(c) N. Ishikawa, M. Sugita, N. Tanaka, T. Ishikawa, S.-Y. Koshihara, Y. Kaizu, Inorg. Chem. 43 (2004) 5498.
[8] (a) M.A. AlDamen, S. Cardona-Serra, J.M. Clemente-Juan, E. Coronado, A. Gaita-Arino, C. Marti-Gastaldo, F. Luis, O. Montero, Inorg. Chem. 48 (2009) 3467;
(b) M.A. AlDamen, J.M. Clemente-Juan, E. Coronado, C. Marti-Gastaldo, A. Gaita-Arino, J. Am. Chem. Soc. 130 (2008) 8874.
[9] (a) S.-D. Jiang, S.-S. Liu, L.-N. Zhou, B.-W. Wang, Z.-M. Wang, S. Gao, Inorg. Chem. 51 (2012) 3079;
(b) S.-D. Jiang, B.-W. Wang, G. Su, Z.-M. Wang, S. Gao, Angew. Chem., Int. Ed. 49 (2010) 7448.
[10] G. Cucinotta, M. Perfetti, J. Luzon, M. Etienne, P.-E. Car, A. Caneschi, G. Calvez, K. Bernot, R. Sessoli, Angew. Chem., Int. Ed. 51 (2012) 1606.
[11] A. Watanabe, A. Yamashita, M. Nakano, T. Yamamura, T. Kajiwara, Chem.-Eur. J. 17 (2011) 7428.
[12] (a) N. Ishikawa, Polyhedron 26 (2007) 2147;
(b) N. Ishikawa, Struct. Bond. 135 (2010) 211;
S. Takamatsu, T. Ishikawa, Inorg. Chem. 46 (2007) 7250.
[13] S. Cardona-Serra, J.M. Clemente-Juan, E. Coronado, A. Gaita-Arino, A. Camon, M. Evangelisti, F. Luis, M.J. Martinez-Perez, J. Sese, J. Am. Chem. Soc. 134 (2012) 14982.
[14] J.J. Baldovi, S. Cardona-Serra, J.M. Clemente-Juan, E. Coronado, A. Gaita-Arino, A. Palii, Inorg. Chem. 51 (2012) 12565.
[15] M.J. Frisch, G.W. Trucks, H.B. Schlegel, G.E. Scuseria, M.A. Robb, J.R. Cheeseman, G. Scalmani, V. Barone, B. Mennucci, G.A. Petersson, H. Nakatsuji, M. Caricato, X. Li, H.P. Hratchian, A.F. Izmaylov, J. Bloino, G. Zheng, J.L. Sonnenberg, M. Hada, M. Ehara, M. Toyota, R. Fukuda, J. Hasegawa, M. Ishida, T. Nakajima, Y. Honda, K. O., H. Nakai, T. Vreven, J.A. Montgomery Jr., J.E. Peralta, F. Ogliaro, M. Bearpark, J.J. Heyd, E. Brothers, K.N. Kudin, V.N. Staroverov, R. Kobayashi, J. Normand, K. Raghavachari, A. Rendell, J.C. Burant, S.S. Iyengar, J. Tomasi, M. Cossi, N. Rega, J.M. Millam, M. Klene, J.E. Knox, J.B. Cross, V. Bakken, C. Adamo, J. Jaramillo, R. Gomperts, R.E. Stratmann, O. Yazyev, A.J. Austin, R. Cammi, C. Pomelli, J.W. Ochterski, R.L. Martin, K. Morokuma, V.G. Zakrzewski, G.A. Voth, P. Salvador, J.J. Dannenberg, S. Dapprich, A.D. Daniels, O. Farkas, J.B. Foresman, J.V. Ortiz, J. Cioslowski, D.J. Fox, Gaussian Inc., Wallingford, CT, 2009.
[16] F. Neese, Comput. Mol. Sci. 2 (2012) 73.

[17] (a) A.D. Becke, Phys. Rev. A: Gen. Phys. 38 (1988) 3098;
(b) A.D. Becke, J. Chem. Phys. 98 (1993) 5648.
[18] A. Schaefer, C. Huber, R. Ahlrichs, J. Chem. Phys. 100 (1994) 5829.
[19] Z. Benko, S. Burck, D. Gudat, M. Nieger, L. Nyulaszi, N. Shore, Dalton Trans. (2008) 4937.
[20] (a) P.-H. Lin, T.J. Burchell, R. Clerac, M. Murugesu, Angew. Chem., Int. Ed. 47 (2008) 8848;
(b) P.-H. Lin, T.J. Burchell, L. Ungur, L.F. Chibotaru, W. Wernsdorfer, M. Murugesu, Angew. Chem., Int. Ed. 48 (2009) 9489;
(c) P.-H. Lin, W.-B. Sun, M.-F. Yu, G.-M. Li, P.-F. Yan, M. Murugesu, Chem. Commun. 47 (2011) 10993.
[21] I.J. Hewitt, J. Tang, N.T. Madhu, C.E. Anson, Y. Lan, J. Luzon, M. Etienne, R. Sessoli, A.K. Powell, Angew. Chem., Int. Ed. 49 (2010) 6352.
[22] J.D. Lee, Concise Inorganic Chemistry, Blackwell Science Ltd., 1996, P. 861.
[23] J. Ruiz, A.J. Mota, A. Rodriguez-Dieguez, S. Titos, J.M. Herrera, E. Ruiz, E. Cremades, J.P. Costes, E. Colacio, Chem. Commun. 48 (2012) 7916.
[24] C. Senol, Z. Hayvali, H. Dal, T. Hoekelek, J. Mol. Struct. 997 (2011) 53.
[25] A. Ewert, K.J. Wannowius, H. Elias, Inorg. Chem. 17 (1978) 1691.
[26] S. Yamada, Coord. Chem. Rev. 1 (1966) 415.
[27] (a) A. Chakravorty, J.P. Fennessey, R.H. Holm, Inorg. Chem. 4 (1965) 26;
(b) L. Sacconi, R. Cini, F. Maggio, J. Inorg. Nucl. Chem. 8 (1958) 489;
(c) L. Sacconi, G. Lombardo, P. Paoletti, J. Chem. Soc. (1958) 848.
[28] S. Yamada, E. Ohno, Y. Kuge, A. Takeuchi, K. Yamanouchi, K. Iwasaki, Coord. Chem. Rev. 3 (1968) 247.
[29] (a) M. Atanasov, P. Comba, G.R. Hanson, S. Hausberg, S. Helmle, H. Wadepohl, Inorg. Chem. 50 (2011) 6890;
(b) D.J. Cookson, T.D. Smith, J.R. Pilbrow, Bull. Chem. Soc. Jpn. 48 (1975) 2832;
(c) M. Eckshtain-Levi, R. Lavi, D. Yufit, M. Orio, R. Wanke, L. Benisvy, Dalton Trans. 41 (2012) 12457;
(d) W.E. Estes, W.E. Hatfield, Inorg. Chem. 17 (1978) 3226;
(e) A.M. Whyte, B. Roach, D.K. Henderson, P.A. Tasker, M.M. Matsushita, K. Awaga, F.J. White, P. Richardson, N. Robertson, Inorg. Chem. 50 (2011) 12867.
[30] (a) M. Brustolon, E. Giamello (Eds.), Electron Paramagnetic Resonance, A Practitioner's Toolkit, 2009; (b) J.A. Weil, J.R. Bolton, Electron paramagnetic resonance, in: John A. Weil, James R. Bolton (Eds.), second ed., Elementary Theory and Practical Applications, 2009; (c) J.E. Wertz, J.R. Bolton, Electron Spin Resonance, Elementary Theory and Practical Applications, McGraw-Hill Series in Advanced Chemistry, 1972.
[31] M. Atanasov, P. Comba, B. Martin, V. Mueller, G. Rajaraman, H. Rohwer, S. Wunderlich, J. Comput. Chem. 27 (2006) 1263.

Please cite this article in press as: A. Upadhyay et al., Polyhedron (2013), http://dx.doi.org/10.1016/j.poly.2013.02.039